Similarity scaling for low-pressure capacitive radio-frequency CF_4 plasmas across operation modes

Zhenhua Zhou [1], Xiaokun Wang [2], Hanyang Li [3], Julian Schulze [2], Peter Hartmann [4], Zoltán Donkó [4], Yongxin Liu [5], and Yangyang Fu [3,6,7,*]

[1]*Department of Engineering Physics, Tsinghua University, Beijing 100084, China*

[2]*Chair of Applied Electrodynamics and Plasma Technology, Faculty of Electrical Engineering and Information Sciences, Ruhr University Bochum, 44801 Bochum, Germany*

[3]*Department of Electrical Engineering, Tsinghua University, Beijing 100084, China*

[4]*Institute for Solid State Physics and Optics, HUN-REN Wigner Research Centre for Physics, 1121 Budapest, Hungary*

[5]*Key Laboratory of Materials Modification by Laser, Ion, and Electron Beams (Ministry of Education), School of Physics, Dalian University of Technology, Dalian 116024, China*

[6]*State Key Laboratory of Power System Operation and Control, Department of Electrical Engineering, Tsinghua University, Beijing 100084, China*

[7]*Sichuan Energy Internet Research Institute, Tsinghua University, Sichuan 610213, China*

(Received 21 October 2025; accepted 15 January 2026; published 9 February 2026)

Similarity laws (SLs) describe how physical characteristics in plasma discharges remain consistent at different dimensional scales, and they have been verified in electropositive capacitively coupled radio-frequency (RF) plasmas across a wide range of discharge conditions. In this work, we explore the properties of similarity scaling in low-pressure CF_4 capacitive RF plasma via fully kinetic particle-in-cell/Monte Carlo collision simulations. We find that under our conditions, the densities of all charged particles exhibit similarity. This property arises as the collision reactions governing the changes in particle density are all linear reactions, whose reaction rates satisfy the SL scaling. The similarity factor of electron density is consistent with classical similarity theory. However, the similarity factor of the density of each ion species deviates consistently from similarity theory. The reason for this deviation across all discharge modes, including striation, drift-ambipolar, and α-modes, is discussed. Furthermore, we show that this similarity property of ion densities constitutes a destruction of discharge similarity in the striation mode. This study improves the understanding of the similarity laws in electronegative RF discharges.

DOI: 10.1103/7z84-ccpw

I. INTRODUCTION

Low-pressure capacitively coupled radio-frequency (RF) plasmas have been extensively studied due to their widespread applications in material processing [1–4]. Optimizing processes based on such plasma sources relies on precise control of discharge parameters, which directly determine plasma properties and processing performance. For example, a higher ion flux reaching the target surface usually leads to a higher etching rate [5]; an elevated electron temperature can enhance the production of reactive species, which influence the efficiency of etching and deposition [6]. Over the past decades, extensive research has been conducted to investigate the scaling dependence of the discharge characteristics on critical control parameters, including the applied RF voltage amplitude V_0 [7–9], gas pressure p [10–12], electrode gap distance d [13–15], and RF driving frequency f [16–19]. However, it is still challenging to study the scaling laws of discharge characteristics with respect to these control parameters, since there are competing physical mechanisms inducing nonlinear transition regimes of the discharge. For example, variations in gas pressure can cause the dominant electron power absorption mechanism to shift between nonlocal collisional heating and Ohmic heating [20]. An increase in the RF driving frequency may cause the discharge to transition from being dominated by electrostatic effects to electromagnetic effects, which eventually introduce significant radial nonuniformity in the discharge [21]. The rise in the applied voltage can enhance the impact of secondary electrons on the discharge, resulting in the transition of the operation mode from the α-mode to the γ-mode [22].

The similarity law (SL) is a powerful tool for predictions of RF discharge characteristics. It reveals that physical principles remain consistent across different dimensional scales. Early researches on gas discharge similarity were pioneered by Townsend [23], Holm [24], Engel [25], Margenau [26], and others [27–29]. The SL has been applied to various discharge types, including glow discharges [30–32], streamers [33,34], pulsed discharges [35], and magnetohydrodynamic plasmas [36]. Regarding RF plasmas, the validity of the similarity law has been confirmed by both experiments [37] and simulations [38–43] in electropositive (e.g., argon) discharges. Under similar conditions, previous work verified the invariance of spatiotemporal plasma characteristics in electropositive capacitive RF discharges across nonlinear transition regimes

*Contact author: fuyangyang@tsinghua.edu.cn

 ©2026 American Physical Society

[42], as well as in the presence of a magnetic field [43] or the electrical asymmetric effect [41].

Investigating the applicability of the similarity laws to RF discharges in electronegative gases (e.g., CF_4 plasmas) is of vital importance, since they play a critical role in plasma processing [44,45] and surface modification [46,47]. Yet, the applicability of similarity laws to electronegative RF discharges still remains unclear due to the reaction complexity of these systems. For example, two unique discharge modes are observed in electronegative RF discharges: striation mode and drift-ambipolar (DA) mode. The striation mode typically arises at a low driving frequency, and it is characterized by the establishment of spatially modulated, "*comb-like*" plasma density structures [48]. These structures are attributed to the ion response to the RF field, where positive and negative ions collectively adjust the local polarity of the space charge [49]. The DA mode is characterized by the drift electric field built in the bulk plasma region due to strong electronegativity, whereas ambipolar electric fields form near sheath boundaries as a result of strong electron density gradients there [22]. Previous studies revealed that the discharge mode of RF discharges in CF_4 will remain invariant when the system is geometrically scaled by a small scaling factor, k (e.g., $k \leqslant 2$); at larger scaling factors, the striation mode transitions toward the DA mode [50]. The existence of nonlinear collisions (the reaction rates of which do not follow the SL scaling) will cause the ion density scaling relation to progressively deviate from similarity predictions as k increases [50]. However, quantitative discussions on the similarity properties of plasma parameters, such as the density of charged particles, still remain insufficient.

In this work, we employ the kinetic particle-in-cell/Monte Carlo collision (PIC/MCC) approach to explore the similarity properties of low-pressure capacitive RF plasmas in CF_4. Under the conditions studied, we find that the spatiotemporal characteristics of each charged species, namely electrons, positive ions, and negative ions, show consistency among similar discharges. This is because the collision reactions that dominate the change in particle density are linear reactions (the reaction rates of which follow the SL scaling), including ion-ion recombination reactions. Additionally, regarding electrons, the scaling factor of electron density is consistent with the similarity theory [51]. However, scaling factors of ion densities deviate quantitatively from the similarity theory. We have verified that this deviation persists across striation, DA, and α-modes. Through theoretical analysis and test-particle trajectory calculations, we have shown that this similarity characteristic of ion densities essentially leads to the breakdown of discharge similarity.

This paper is organized as follows. In Sec. II, the simulation model and the calculation method are introduced. Section III provides the simulation results and the corresponding discussions. Finally, conclusions are drawn in Sec. IV.

II. MODEL AND METHOD

The SL provides a powerful analytical approach to parameter scaling. The SL theory asserts that, in a pair of similar discharge systems, a physical parameter G at the spatiotemporal point (x_1, t_1) can be expressed in terms of its scaled counterpart (x_k, t_k) using the similarity relation

$$G(x_1, t_1) = k^{\alpha[G]} G(x_k, t_k), \tag{1}$$

where $k = x_1/x_k = t_1/t_k$ is the scaling factor, and $\alpha[G]$ is the similarity factor for parameter G [42]. For typical RF discharge, the control parameters $[p,\ d,\ f]$ should be scaled as $k = p_k/p_1 = d_1/d_k = f_k/f_1$ for similar discharges, keeping f/p and pd unchanged. Therefore, $\alpha[p] = -1$, $\alpha[d] = 1$, and $\alpha[f] = -1$ for the pressure, gap distance, and driving frequency, respectively. Typically, for the electron density n_e and the electron current density $\mathbf{J}_e$, the similarity factors are verified to satisfy $\alpha[n_e] = \alpha[\mathbf{J}_e] = -2$ [52]. For the electric field, $\alpha[\mathbf{E}] = -1$. Additionally, parameters satisfying $\alpha[G] = 0$ are called similarity invariants, including the electron energy $\mathcal{E}_e$, electron temperature T_e, electron mean velocity u_e, and electric potential ϕ. Furthermore, all rate coefficients utilized in our simulation are also similarity invariants, since they are merely functions of similarity invariants, T_e and T_i. Note that similar factors as described above for the electrons also apply to ions, i.e., $\alpha[n_e] = \alpha[n_i] = -2$ and $\alpha[T_e] = \alpha[T_i] = 0$.

Considering $\alpha[n] = -2$ for the density of any charged species and $\alpha[t] = -1$ for time, the temporal change of the density satisfies

$$\left(\frac{\partial n}{\partial t}\right)_1 = k^{-3}\left(\frac{\partial n}{\partial t}\right)_k. \tag{2}$$

In other words, only if $\alpha[\partial n/\partial t] = -3$ will the SL scaling hold for the density of this species [35,53]. Therefore, if the reaction rate R of a collision process inducing particle density change follows $\alpha[R] = -3$, it is classified as a linear collision. A typical example is the one-step electron impact ionization process. Its reaction rate, R_{iz}, is given as

$$R_{iz} = K_{iz} n_e n_g, \tag{3}$$

where K_{iz}, as a function of T_e, is the ionization rate coefficient. As $\alpha[K_{iz}] = \alpha[T_e] = 0$, $\alpha[n_e] = -2$, and $\alpha[n_g] = -1$, we have $\alpha[R_{iz}] = -3$, behaving as a linear collision process. On the other hand, the nonlinear collision process can cause a deviation from the SL scaling of the particle density. The reaction rate of a nonlinear process does not adhere to the similarity factor of -3, such as electron-ion recombination [53].

TABLE I. Discharge conditions and the corresponding discharge mode of the base case with $k = 1$.

Case no.	$[p_1, d_1, f_1]$	Discharge mode
1	[60 Pa, 2 cm, 6.78 MHz]	Striation
2	[60 Pa, 2 cm, 13.56 MHz]	Drift-ambipolar
3	[60 Pa, 2 cm, 54.24 MHz]	Alpha

The results in this study are based on an electrostatic PIC/MCC code in 1d3v, which is validated against experiment [54]. In the typical parallel electrode geometry, the powered electrode is driven by an RF voltage source $V_0\cos(2\pi f t)$, where $V_0 = 300$ V. The grounded electrode is placed at the opposite side. The background gas is assumed to be uniform and at a temperature of $T_g = 350$ K having a Maxwellian distribution. The discharge conditions, including CF_4 gas

TABLE II. Electron-neutral collisions considered in the simulation.

No.	Reaction	Type
R1	$e + CF_4 \rightarrow e + CF_4$	Elastic scattering
R2	$e + CF_4 \rightarrow e + CF_4(v = 1)$	Vib. excitation
R3	$e + CF_4 \rightarrow e + CF_4(v = 3)$	Vib. excitation
R4	$e + CF_4 \rightarrow e + CF_4(v = 4)$	Vib. excitation
R5	$e + CF_4 \rightarrow e + CF^*$	Excitation
R6	$e + CF_4 \rightarrow 3e + CF_3^+ + F$	Diss. ionization
R7	$e + CF_4 \rightarrow 2e + CF_2^+ + F$	Diss. ionization
R8	$e + CF_4 \rightarrow 3e + CF_3^{2+} + 2F$	Diss. ionization
R9	$e + CF_4 \rightarrow 2e + CF^+ + 2F$	Diss. ionization
R10	$e + CF_4 \rightarrow 2e + CF^+ + 3F$	Diss. ionization
R11	$e + CF_4 \rightarrow 2e + C^+ + 4F$	Diss. ionization
R12	$e + CF_4 \rightarrow 2e + F^+ + CF_3$	Diss. ionization
R13	$e + CF_4 \rightarrow F^- + CF_3$	Attachment
R14	$e + CF_4 \rightarrow F + CF_3^-$	Attachment
R15	$e + CF_4 \rightarrow e + F + CF_3$	Dissociation
R16	$e + CF_4 \rightarrow e + 2F + CF_2$	Dissociation
R17	$e + CF_4 \rightarrow e + 3F + CF$	Dissociation

pressure p_1, gap distance d_1, and driving frequency f_1, along with the corresponding discharge modes of our base cases ($k = 1$), are outlined in Table I. For each case, simulations for the scaled system with $[p_k, d_k, f_k] = [kp_1, d_1/k, kf_1]$ ($k = 2$) are also performed. Surface interactions include elastic electron reflection (coefficient $\delta_{\text{ref}} = 0.7$) and secondary electron emission (coefficient $\gamma_{\text{see}} = 0.01$) induced by positive ion bombardment at both electrodes [54]. To ensure simulation stability and accuracy, a spatial resolution of $\Delta x = d/1000$ and a temporal resolution of $\Delta t = 1/8000f$ are applied. The reactions between electrons and neutral gas considered in the simulation, along with their reaction types, are listed in Table II. The abbreviations Diss. and Vib. stand for dissociative and vibrational, respectively. Ion-neutral reactions are provided in Table III. Elastic collisions can be classified as either isotropic or anisotropic angular scattering [55]. The other reactions are classified according to the following rules: (a) "Reactive (keep ion type)": the reaction produces an ion of the same type as the reactant ion. (b) "Reactive (change ion type)": the reaction produces an ion that is different from the reactant ion. (c) "Detachment": the reaction produces an electron. It should be noted that for R21, R30, and R31, these reactions produce minority ionic species that are not considered in the model. For simplicity, the product ions of these reactions are treated as identical to the reactants. A detailed description of this treatment can be found in Ref. [54].

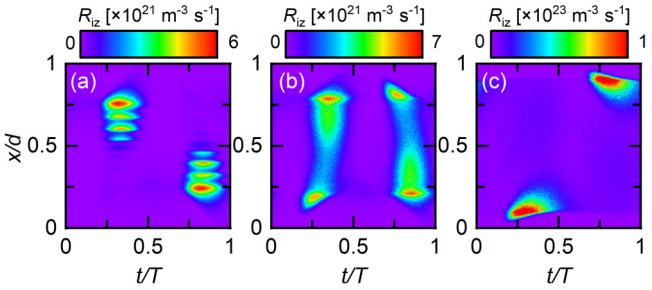


FIG. 1. Spatiotemporal distributions of the reaction rate of electron impact dissociative ionization (producing CF_3^+) obtained in (a) case 1, (b) case 2, and (c) case 3, presenting typical characteristics of the striation mode, drift-ambipolar (DA) mode, and α-mode, respectively.

III. RESULTS AND DISCUSSION

Figure 1 presents the spatiotemporally resolved reaction rate of electron impact dissociative ionization generating CF_3^+. Panels (a), (b), and (c), respectively, present the results obtained in case 1, case 2, and case 3, whereas three distinct discharge modes are involved: the striation mode, the DA mode, and the α-mode, respectively. The striation mode and the DA mode have been reported as two specific modes in electronegative RF discharges [22,48]. Panel (a) shows that the ionization rate exhibits a spatially modulated structure, featuring the striation mode discharge. Panel (b) presents a distinct distribution of the ionization rate in the bulk region, corresponding to the drift electric field established by the strong electronegativity in the DA mode. In panel (c), there are significant ionization rate peaks during sheath expansion phases, which is consistent with the characteristics of electron

TABLE III. Ion-neutral collisions considered in the simulation [54].

No.	Reaction	Type
R18	$CF_3^+ + CF_4 \rightarrow CF_3^+ + CF_4$	Elastic scattering
R19	$CF_3^+ + CF_4 \rightarrow CF_3^+ + CF_3 + F$	Reactive (keep ion type)
R20	$CF_3^+ + CF_4 \rightarrow CF_2^+ + CF_4 + F$	Reactive (change ion type)
R21	$CF_3^+ + CF_4 \rightarrow CF_3^+ +$ others	Reactive (keep ion type)
R22	$CF_2^+ + CF_4 \rightarrow CF_2^+ + CF_4$	Elastic scattering
R23	$CF_2^+ + CF_4 \rightarrow e + F + CF_3^+ + CF_4$	Detachment
R24	$CF_2^+ + CF_4 \rightarrow CF_2^+ + CF_3 + F$	Reactive (keep ion type)
R25	$CF_2^+ + CF_4 \rightarrow CF^+ + CF_4 + F^-$	Reactive (change ion type)
R26	$F^- + CF_4 \rightarrow F^- + CF_4$	Elastic scattering
R27	$F^- + CF_4 \rightarrow e + F + CF_4$	Detachment
R28	$F^- + CF_4 \rightarrow F + F^- + CF_3$	Reactive (keep ion type)
R29	$CF^+ + CF_4 \rightarrow CF^+ + CF_4$	Elastic scattering
R30	$CF^+ + CF_4 \rightarrow CF^+ +$ others	Reactive (keep ion type)
R31	$CF^+ + CF_4 \rightarrow$ others	Reactive (keep ion type)

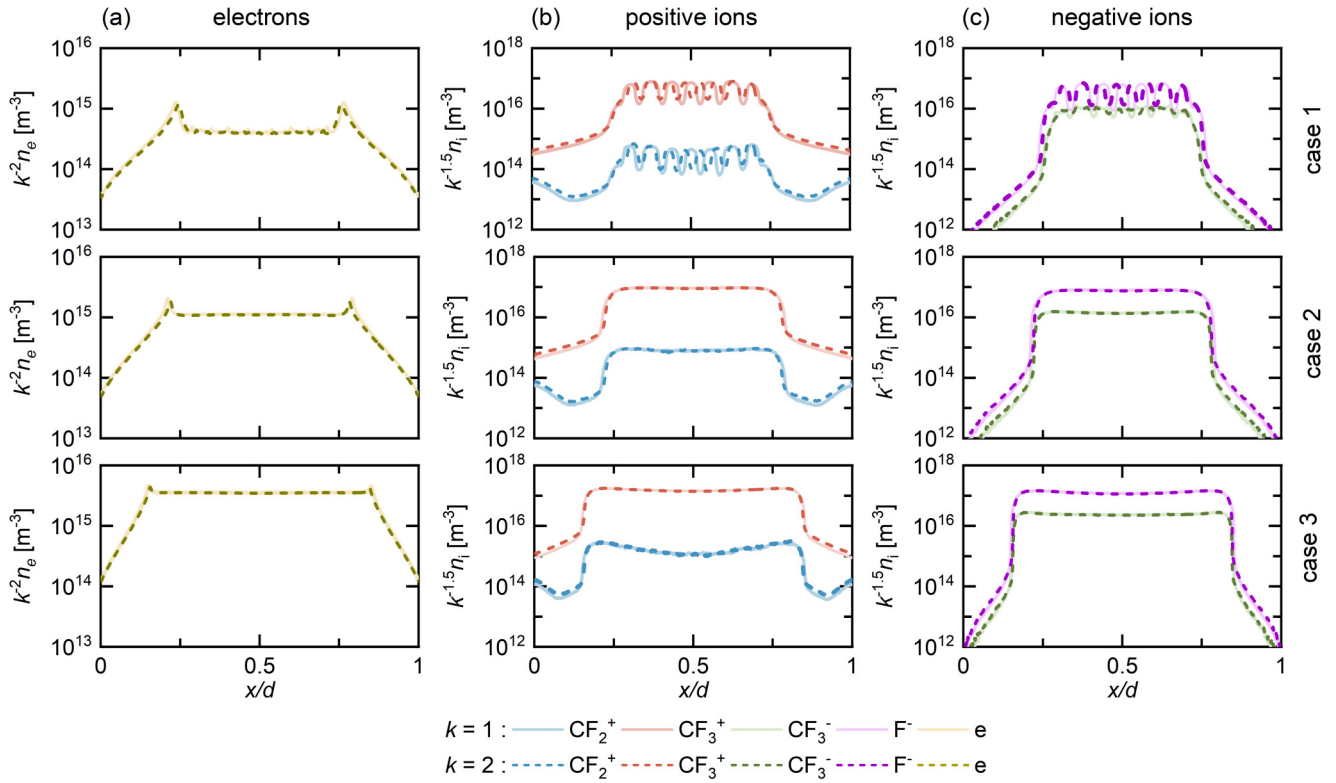


FIG. 2. RF period-averaged profiles of scaled particle densities obtained in case 1 (first row), case 2 (second row), and case 3 (third row). The solid and dashed lines represent the results obtained in the base case ($k = 1$) and the similar case ($k = 2$), respectively. The densities are scaled by k^{-2} in panel (a) for electrons, and by $k^{-1.5}$ in panels (b) and (c) for positive and negative ions, respectively. All results present good overlap.

power absorption in the α-mode. Covering these representative discharge modes ensures that the conclusions drawn in this work are independent of any particular discharge mode.

Figure 2 shows the RF period-averaged profiles of scaled charged particle densities, where the first, second, and third rows, respectively, correspond to results obtained in case 1, case 2, and case 3. The solid lines show the results obtained in the base cases, while the dashed lines correspond to the similar cases. In panel (a), the electron densities are scaled by k^{-2}. Here, the similarity factor of -2 is given by the classical SL theory. However, in panels (b) and (c), the positive and negative ion densities are scaled by $k^{-1.5}$ and the profiles still exhibit overlapping. This property is independent of the discharge mode and ion species. To further demonstrate this invariance, we calculate the similarity factor from the simulation results via

$$\alpha[n] = \log_k\left(\frac{\langle n_1(x,t)\rangle}{\langle n_k(x,t)\rangle}\right), \tag{4}$$

where $\langle n_k(x,t)\rangle$ and $\langle n_1(x,t)\rangle$ are the spatiotemporally averaged densities in the similar and base cases, respectively. According to Eq. (4), the similarity factors of each charged species are determined in Table IV. It is further illustrated that the density of each ion species has a scaling factor of approximately -1.5, deviating from the similarity prediction, -2 [51]. This deviation holds across different discharge modes. Here, we provide a qualitative clarification for the property of $\alpha[n_i] = -1.5$. Table V presents the recombination reactions and corresponding rate coefficients. The reaction rates of the three involving CF_3^+ ions, i.e., Re1, Re2, and Re3, are labeled as R_{rec1}, R_{rec2}, and R_{rec3}, respectively. The reaction rates of those involving the CF_2^+ ions are negligible compared to those involving the CF_3^+ ions, thus they are not discussed here. For the two ion-ion recombination reactions, we have

$$\alpha[R_{rec2}] = \alpha[K_{rec2}] + \alpha[n_{CF_3^+}] + \alpha[n_{F^-}] \tag{5}$$

and

$$\alpha[R_{rec3}] = \alpha[K_{rec3}] + \alpha[n_{CF_3^+}] + \alpha[n_{CF_3^-}]. \tag{6}$$

According to Table V, the similarity factors of the rate coefficients satisfy

$$\alpha[K_{rec2}] = \alpha[K_{rec3}] = 0. \tag{7}$$

Additionally, as predicted by similarity theory, the densities of all ions share a common similarity factor

$$\alpha[n_{CF_3^+}] = \alpha[n_{CF_3^-}] = \alpha[n_{F^-}] = \alpha[n_i]. \tag{8}$$

TABLE IV. Similarity factors for spatiotemporally averaged densities of different charged particles.

Case no.	$\alpha[n_{CF_2^+}]$	$\alpha[n_{CF_3^+}]$	$\alpha[n_{CF_3^-}]$	$\alpha[n_{F^-}]$	$\alpha[n_e]$
1	−1.52	−1.51	−1.50	−1.49	−1.93
2	−1.48	−1.45	−1.45	−1.44	−1.93
3	−1.58	−1.47	−1.47	−1.44	−1.95

TABLE V. Recombination processes considered in the simulation with the corresponding rate coefficients. The ion and electron temperatures, T_i and T_e, are in units of eV.

No.	Reaction	Rate coefficient ($m^3\ s^{-1}$)
Re1	$e + CF_3^+$	$3.95 \times 10^{-15}\ T_e^{-0.5}$
Re2	$F^- + CF_3^+$	1×10^{-13}
Re3	$CF_3^- + CF_3^+$	1×10^{-13}
Re4	$e + CF_2^+$	$3.95 \times 10^{-15}\ T_e^{-0.5}$
Re5	$F^- + CF_2^+$	1×10^{-13}
Re6	$CF_3^- + CF_2^+$	1×10^{-13}

Combining Eqs. (5), (6), (7), and (8), we have

$$\alpha[R_{\mathrm{rec2}}] = 2\alpha[n_i] \tag{9}$$

and

$$\alpha[R_{\mathrm{rec3}}] = 2\alpha[n_i]. \tag{10}$$

According to Eqs. (9) and (10), $\alpha[n_i] = -1.5$ originates from $\alpha[R_{\mathrm{rec2}}] = \alpha[R_{\mathrm{rec3}}] = -3$. That is, in electronegative RF discharges, ion-ion recombination reactions (primarily CF_3^+ with F^- and CF_3^+ with CF_3^-) must behave as linear collision processes. To clarify, we assume all ion-ion recombination reactions to be linear collision processes. Thus, the densities of F^- ions and CF_3^+ ions will both satisfy similarity scaling, i.e.,

$$n_{F^-,1} = k^a n_{F^-,k} \tag{11}$$

and

$$n_{CF_3^+,1} = k^b n_{CF_3^+,k}, \tag{12}$$

where a and b represent the similarity factors for the densities of F^- and CF_3^+ ions, and they are both equal to -1.5. Equations (11) and (12) hold because, besides ion-ion recombination, the other collision reactions affecting the densities of the two species are dominated by linear processes.

Additionally, for CF_4 capacitive RF discharges, since the quasineutrality is mainly maintained by CF_3^+ and F^- ions [56], their densities in the base case and the similar case should satisfy, respectively,

$$n_{F^-,1} = n_{CF_3^+,1} \tag{13}$$

and

$$n_{F^-,k} = n_{CF_3^+,k}. \tag{14}$$

Equations (11) and (12) self-consistently support the quasineutrality [Eqs. (13) and (14)], indicating that ion-ion recombination reactions are required to be linear collision processes in electronegative RF discharges. If they are nonlinear collisions, then CF_3^+ ions will experience a higher density loss rate than F^- ions in similar systems, as they are involved in a different number of recombination reactions. This leads to $a \neq b$ in Eqs. (11) and (12), and the quasineutrality will not be self-consistently satisfied. However, the electron-ion recombination is classified as a nonlinear process since its similarity factor satisfies $\alpha[R_{\mathrm{rec1}}] = \alpha[K_{\mathrm{rec1}}] + \alpha[n_e] + \alpha[n_i] = -3.5$, which deviates from $\alpha[\partial n/\partial t] = -3$. Since the electron density is much lower than the ion density, the electron-ion recombination does not cause an obvious violation of the similarity scaling in the present work.

We take the F^- ion as the representative ion for the following discussions, since this species is present at the highest density among negatively charged particles. The spatiotemporal distributions of the scaled electron density, $k^{-2}n_e$, and F^- ion density, $k^{-1.5}n_{F^-}$, are presented in Fig. 3. In the first row, panels (a1) and (b1), respectively, show n_e and n_{F^-} obtained in case 1, where panels (c1),(d1) and (e1),(f1) correspondingly present the results obtained in cases 2 and 3. In the second row, panels (a2)–(f2) present the scaled densities of the corresponding similar cases ($k = 2$), sharing the identical color bars with the first row. It can be observed that the scaled densities exhibit similarity, including the spatiotemporal characteristics and magnitude. This consistency is independent of the discharge operation mode. Notably, though the scaled densities in case 1 demonstrate quantitative agreement, the number of striations differs, as there are seven density peaks in panel (b1) and eight in panel (b2). To clarify this difference, as the spatially modulated structure arises from the oscillation of positive and negative ions, we introduce the equation describing the relative ion displacement during the oscillation, proposed in Ref. [49]:

$$x(t) = \frac{eE_0\ /\ \mu_m}{\sqrt{\left(\omega_{rf}^2 - \omega_i^2\right)^2 + \omega_{rf}^2 \nu_c^2}} \sin(\omega_{rf} t - \varphi), \tag{15}$$

where e is the unit charge, E_0 is the bulk electric field amplitude, ν_c is the ion collision frequency, $\omega_{rf} = 2\pi f$ is the RF angular driving frequency, φ is the oscillation phase shift, and μ_m is the reduced mass of the positive and negative ions, which is dependent on the gas type and can be treated as a constant. The eigenfrequency of the ion oscillation, ω_i, is defined as [49]

$$\omega_i^2 = \frac{e^2 n_i}{\varepsilon_0 \mu_m}, \tag{16}$$

where n_i is the ion density. From Eq. (15), the amplitude of the oscillation is [49]

$$A = \frac{eE_0\ /\ \mu_m}{\sqrt{\left(\omega_{rf}^2 - \omega_i^2\right)^2 + \omega_{rf}^2 \nu_c^2}}. \tag{17}$$

Then, an approximation to the number of striations in the base case, $N_{str,1}$, can be obtained by dividing the width of the bulk plasma region, L, by the amplitude A:

$$N_{str,1} = \frac{L}{A} = \frac{L\sqrt{\left(\omega_{rf}^2 - \omega_i^2\right)^2 + \omega_{rf}^2 \nu_c^2}}{eE_0\ /\ \mu_m}. \tag{18}$$

In Eq. (18), the bulk plasma width can be considered to have the same similarity factor as the gap distance, d, i.e., $\alpha[L] = \alpha[d] = 1$. This can be confirmed visually in panels (a1) and (a2), in which the range of both bulk regions is approximately $0.25d$ to $0.75d$. Regarding the driving frequency, there is $\alpha[\omega_{rf}^2] = \alpha[f^2] = -2$; the ion collision frequency, ν_c, can be assumed to be proportional to the gas pressure, $\alpha[\nu_c^2] = \alpha[p^2] = -2$, and we have $\alpha[E_0] = -1$ for the field amplitude. Finally, if $\alpha[n_i] = -2$, then $\alpha[\omega_i] = -2$ according to Eq. (16). Overall, by applying the above scaling relationships, the number of striations in the similar case, $N_{str,k}$, can

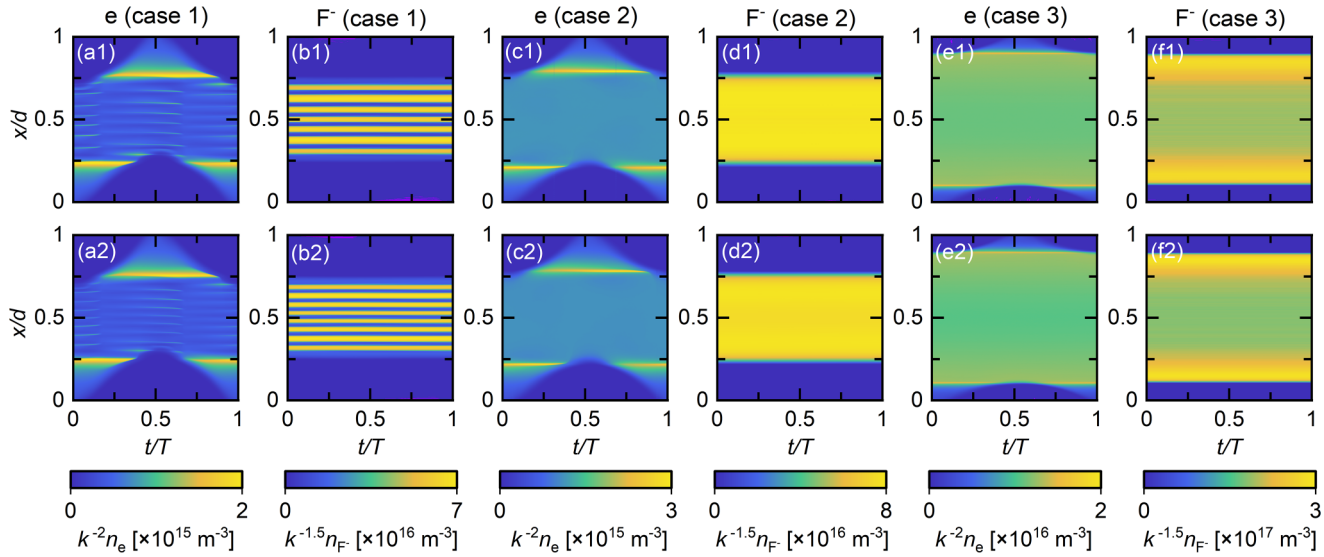


FIG. 3. Spatiotemporal distribution of the scaled (a) electron density and (b) F^- ion density obtained in case 1, (c) electron density and (d) F^- ion density obtained in case 2, and (e) electron density and (f) F^- ion density obtained in case 3. The first row [(a1)−(f1)] and the second row [(a2)−(f2)] present the results obtained in the base case ($k = 1$) and the similar case ($k = 2$), respectively. Here, n_e is scaled by k^{-2}, and n_{F^-} is scaled by $k^{-1.5}$.

be expressed as

$$N_{\mathrm{str},k} = \frac{kL\sqrt{\left[\left(k^{-2}\omega_{\mathrm{rf}}^2\right) - \left(k^{-2}\omega_{\mathrm{i}}^2\right)\right]^2 + \left(k^{-2}\omega_{\mathrm{rf}}^2\right)\left(k^{-2}\nu_{\mathrm{c}}^2\right)}}{e(k^{-1}E_0)/\mu_{\mathrm{m}}}$$
$$= \frac{L\sqrt{\left(\omega_{\mathrm{rf}}^2 - \omega_{\mathrm{i}}^2\right)^2 + \omega_{\mathrm{rf}}^2\nu_{\mathrm{c}}^2}}{eE_0/\mu_{\mathrm{m}}}$$
$$= N_{\mathrm{str},1}. \tag{19}$$

That is, ideally, if $\alpha[n_{\mathrm{i}}] = -2$, the number of striations will be constant in similar discharges. However, since it is verified that $\alpha[n_{\mathrm{i}}] = -1.5$, there is $N_{\mathrm{str},k} > N_{\mathrm{str},1}$ in practice. In other words, Eq. (19) reveals that this property of $\alpha[n_{\mathrm{i}}] = -1.5$ essentially constitutes a destruction of discharge similarity. This is also consistent with the similarity theory, which states that for similarity scaling to hold between two discharge systems, $\alpha[n_{\mathrm{i}}] = -2$ must be satisfied.

The dominance of linear collision processes in the density variation of a charged species reveals if its density similarity is maintained. Here, we define R6, R13, and R13 in Table II as G_{e}, L_{e}, and G_{F^-}, and Re2 in Table V as L_{F^-}. These are representative reactions of electron generation and loss, as well as F^- ion generation and loss reactions. The notation G represents particle generation, and L represents loss. Their reaction rates are found to be at least one order of magnitude larger than other reactions of the same type (i.e., the generation or loss of particles). For example, the reaction rate of G_{e} (R6) is about two orders of magnitude larger than R7. Dissociative ionization, G_{e}, is a linear collision maintaining electron density similarity. This is because the summation of the similarity factor of the density of its reactants is -3. Attachment, as both L_{e} and G_{F^-}, has the same reactants as G_{e}, so it is also a linear collision process and maintains similarity of F^- ion density. L_{F^-} is the recombination between F^- with CF_3^+. Its reaction rate similarity factor is -3, behaving as a linear collision process.

Additionally, it should be noted that there are various types of nonlinear collision processes. For example, all detachment reactions producing electrons, i.e., R23 and R27 in Table II, have the similarity factor of $\alpha[R_{\mathrm{det}}] = \alpha[K_{\mathrm{det}}] + \alpha[n_{\mathrm{i}}] + \alpha[n_{\mathrm{g}}] = -2.5$. As for the electron-ion recombination, i.e., Re1 in Table V, there is $\alpha[R_{\mathrm{rec1}}] = \alpha[K_{\mathrm{rec1}}] + \alpha[n_{\mathrm{e}}] + \alpha[n_{\mathrm{i}}] = -3.5$. They deviate from $\alpha[\partial n/\partial t] = -3$ and behave as nonlinear collision processes. However, their reaction rates are negligible compared to the above four reactions (i.e., G_{e}, L_{e}, G_{F^-}, and L_{F^-}), thus their impact on the discharge similarity is minor.

Figure 4 presents the RF period-averaged profiles of the scaled reaction rates, $k^{-3}R$, of the four reactions dominating the generation and loss of electrons and F^- ions, namely G_{e}, L_{e}, G_{F^-}, and L_{F^-}. In the first column, panels (a), (c), and (e) are for G_{e}, L_{e} in cases 1, 2, and 3, and the second column corresponds to G_{F^-} and L_{F^-}. The solid and dashed lines are results obtained in the base case ($k = 1$) and scaled case ($k = 2$). The figure demonstrates that, after scaling by k^{-3}, the profile of reaction rates of G_{e}, L_{e}, G_{F^-}, and L_{F^-} across similar discharges is overlapping, behaving as linear collision processes as defined in Eq. (2). Since linear collision processes dominate the density change of electrons and F^- ions, the similarity scaling is valid for both species, as shown in Figs. 2 and 3.

The effect of a varying driving frequency, f, is presented in Fig. 5 for the spatiotemporally averaged value of (a) the scaled electron and F^- ion density, (b) the scaled reaction rate of G_{F^-} and L_{F^-}, and (c) the scaled reaction rate of G_{e} and L_{e}. Of the five data points, the first denotes striation mode; the second to third denote DA mode; and the fourth to fifth denote α-mode. Across all these modes, the SL predictions match the densities of both electrons and F^- ions shown in panel (a). In panel (b), the scaled reaction rates of G_{F^-} and L_{F^-} consistently exhibit

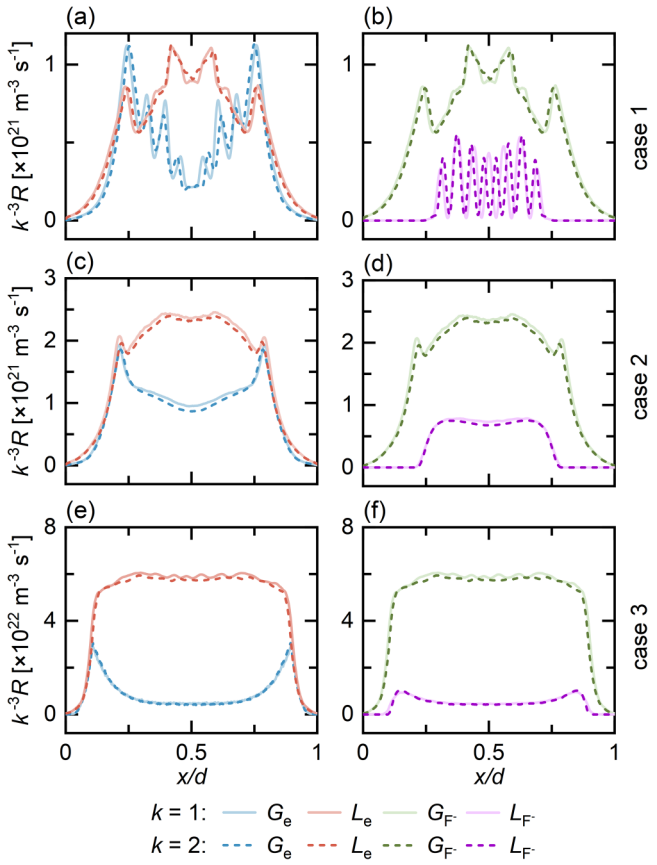


FIG. 4. RF period-averaged profiles of scaled reaction rates ($k^{-3}R$) of G_e, L_e (the first column) and G_{F^-}, L_{F^-} (the second column) in cases 1 − 3.

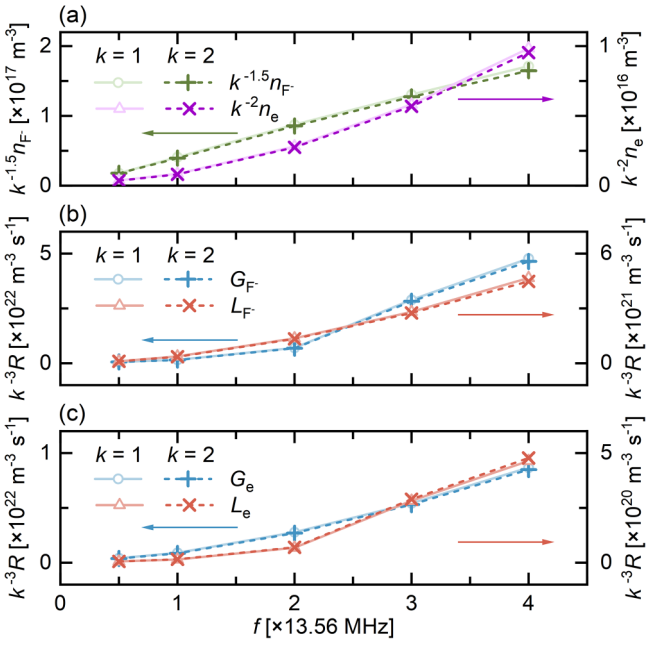


FIG. 5. Spatiotemporally averaged (a) scaled electron and F^- ion density, (b) scaled reaction rate of the primary collision process inducing F^- ion generation, G_{F^-}, and loss, L_{F^-}, and (c) scaled reaction rate of the primary collision process inducing electron generation, G_e, and loss, L_e, as functions of the driving frequency f. Of the five data points in each panel, the first represents striation mode discharge; the second and third represent DA mode; and the fourth and fifth represent α-mode.

good agreement across driving frequencies, behaving as linear collision processes. This confirms the agreement of the scaled F^- ion density in similar discharges. In panel (c), the scaled reaction rates of both G_e and L_e are overlapping, which also supports the maintenance of SL scaling for electron density in panel (a). Overall, Fig. 5 confirms the generality of discharge similarity over a wide range of driving frequencies for CF_4 capacitive RF discharges.

As discussed in the description of Eq. (19), the characteristic of $\alpha[n_i] = -1.5$ is actually a violation of the discharge similarity. Figure 6 further illustrates this feature. The color maps in panels (a), (b), and (c) present the spatiotemporally resolved scaled electric field $k^{-1}E$ obtained from case 1, case 2, and case 3. Panels (a1)–(c1) are results obtained from the base case, where panels (a2)–(c2) are from the corresponding similar cases. Based on the electric field obtained in simulation, we apply the test particle trajectory calculation here [43,57]. This approach determines the trajectory of a test electron with the initial condition (x_0, t_0, v_0). It solves Newton's equation at each time step, ignoring collisions and thermal motion. The colored lines denote electron trajectories, where the color variation reflects the evolution of electron kinetic energy, $\mathcal{E}_{ek}$, along the trajectories. As observed, in panels (b1),(b2) and (c1),(c2), the SL scaling is rigorously valid for both DA mode and α-mode. The spatiotemporal distributions and intensities of the scaled electric field, along

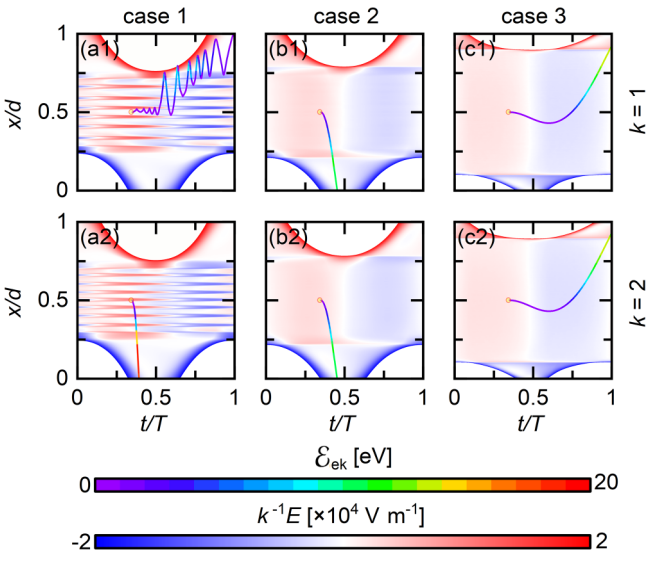


FIG. 6. Spatiotemporal evolution of the scaled electric field, $k^{-1}E$, and the corresponding test electron trajectory departing at $(x_0, t_0, v_0) = (0.5d, 0.35T, 0)$ of (a) case 1, (b) case 2, and (c) case 3. Panels (a1)–(c1) illustrate results from the base cases, and panels (a2)–(c2) present those from the similar cases. Through test particle trajectory calculation, the electron kinetic energy, $\mathcal{E}_{ek}$, is also drawn along the trajectory in a color-coded plot.

with the electron trajectories within the field, exhibit good agreement. However, a distinct difference can be found between panels (a1) and (a2). In (a1), the test electron undergoes multiple rebounds within the spatially modulated electric field before exiting the striation region, and then reaches the plasma-sheath boundary. Subsequently, it undergoes rebound processes between the bulk plasma and sheath edge. The mechanism of this rebound process has been discussed in Ref. [58]; it primarily occurs at the positive and negative polarity transition of the spatially modulated electric field, which mainly traps low-energy electrons. In panel (a2), the test electron can traverse the bulk plasma region and directly reaches the boundary, where it is absorbed. As mentioned earlier, this difference stems directly from the different number of striations resulting from the property of $\alpha[n_i] = -1.5$. Furthermore, for the same initial position $(x_0, t_0) = (0.5d, 0.35T)$, in the base case [panel (a1)] this point may coincide with the transition moment of the positive and negative polarity electric fields, inducing electron confinement there. In contrast, for the similar case [panel (a2)], this point corresponds to the location of maximum electric field intensity among striations. This causes electrons originating from this point to accelerate and remain unconfined by the spatially modulated electric field. Overall, Fig. 6 again demonstrates that the property of $\alpha[n_i] = -1.5$ is essentially a deviation of discharge similarity. This is not in conflict with the existing theory, which indicates that $\alpha[n_i] = -2$ must be satisfied for discharge similarity to hold.

IV. CONCLUSION

In conclusion, we investigated the similarity scaling properties in the low-pressure CF_4 capacitive RF plasmas using the kinetic PIC/MCC collision approach. Through analysis on the RF period-averaged and spatiotemporally resolved characteristics of charged particle density, we confirmed the validity of the SL scaling relations for the electron density under the conditions studied, satisfying $\alpha[n_e] = -2$ as in agreement with the similarity theory. However, although the scaled ion densities overlap as well, we demonstrate that the similarity factor of ion density is -1.5, which is independent of the ion species. This similarity property of ion density violates the classical similarity theory that predicts $\alpha[n_i] = -2$. This violation is attributed to the difference in the number of ion-ion recombination collision types involving CF_3^+ and F^-, whereas both are required to maintain the quasineutrality in both the base case and the similar case. Through a comparative analysis of the collisions, we revealed that the reactions governing variations in electron and F^- ion densities are linear collision reactions, which support the validity of the SL scaling for densities of both species. The above results are observed across distinct discharge modes, including striation mode, DA mode, and α-mode. Moreover, this property of $\alpha[n_i] = -1.5$ is confirmed to be a destruction of the discharge similarity in the striation mode, since it is theoretically revealed to induce a difference in the number of striations. Consequently, the motion of electrons in the striation mode is different between the base case and the similar case, as demonstrated by the test particle calculation. Note that the proposed similarity relations are demonstrated in the representative electronegative gas CF_4, whereas the universality of similarity scalings in various gases still needs investigation in future work.

ACKNOWLEDGMENTS

This work was supported by the National Natural Science Foundation of China (Grant No. U25A6025). The authors also acknowledge financial support from the National Natural Science Foundation of China (Grants No. 52277154 and No. 52250051), the Beijing Natural Science Foundation of China (Grant No. 3244040), and the Organized Research Support Program (Grant No. YK20240103) from the Department of Electrical Engineering at Tsinghua University. X.W. (Project No. 327886311) and J.S. (Project No. 428942393) acknowledge the support of the German Research Foundation.

The authors have no conflicts of interest to disclose.

DATA AVAILABILITY

The data that support the findings of this article are not publicly available. The data are available from the authors upon reasonable request.

[1] I. D. Kaganovich, B. N. Ramamurthi, and D. J. Economou, Self-trapping of negative ions due to electron detachment in the afterglow of electronegative gas plasmas, Appl. Phys. Lett. **76**, 2844 (2000).

[2] T. Makabe and Z. Petrovic, *Plasma Electronics: Applications in Microelectronic Device Fabrication* (CRC, Taylor & Francis Group, Boca Raton, FL, 2014).

[3] P. Chabert and N. Braithwaite, *Physics of Radio-Frequency Plasmas* (Cambridge University Press, Cambridge, 2011).

[4] E. Kessels, A. Devi, J.-S. Park, M. Ritala, A. Yanguas-Gil, and C. Wiemer, Atomic layer deposition, Nat. Rev. Methods Primers **5**, 66 (2025).

[5] W. Jeong, S. Kim, Y. Lee, C. Cho, I. Seong, Y. You, M. Choi, J. Lee, Y. Seol, and S. You, Contribution of ion energy and flux on high-aspect ratio SiO_2 etching characteristics in a dual-frequency capacitively coupled Ar/C_4F_8 plasma: Individual ion energy and flux controlled, Materials **16**, 3820 (2023).

[6] M. Hori, Radical-controlled plasma processes, Rev. Mod. Plasma Phys. **6**, 36 (2022).

[7] T. H. Chung, H. S. Yoon, and J. K. Lee, Scaling laws verification for capacitive rf-discharge Ar plasma using particle-in-cell simulations, J. Appl. Phys. **78**, 6441 (1995).

[8] Y.-R. Zhang, X. Xu, S.-X. Zhao, A. Bogaerts, and Y.-N. Wang, Comparison of electrostatic and electromagnetic simulations for very high frequency plasmas, Phys. Plasmas **17**, 113512 (2010).

[9] V. A. Godyak, R. B. Piejak, and B. M. Alexandrovich, Ion flux and ion power losses at the electrode sheaths in a symmetrical rf discharge, J. Appl. Phys. **69**, 3455 (1991).

[10] G. Q. Yin, J. J. Wang, and Q. H. Yuan, The discharge characteristics of capacitively coupled Ar plasma as the change of pressure, Plasma Phys. Rep. **49**, 802 (2023).
[11] Y.-S. Liang, Y.-X. Liu, Y.-R. Zhang, and Y.-N. Wang, Fluid simulation and experimental validation of plasma radial uniformity in 60 MHz capacitively coupled nitrogen discharges, J. Appl. Phys. **117**, 083301 (2015).
[12] S. K. Babu, S. Kelly, S. Kechkar, P. Swift, S. Daniels, and M. M. Turner, Experimental investigation of electron heating modes in capacitively coupled radio-frequency oxygen discharge, Plasma Sources Sci. Technol. **28**, 115008 (2019).
[13] K. Bera, S. Rauf, K. Ramaswamy, and K. Collins, Effects of interelectrode gap on high frequency and very high frequency capacitively coupled plasmas, J. Vac. Sci. Technol. A **27**, 706 (2009).
[14] Y. Fu, P. Zhang, J. P. Verboncoeur, and X. Wang, Electrical breakdown from macro to micro/nano scales: A tutorial and a review of the state of the art, Plasma Res. Express **2**, 013001 (2020).
[15] A. M. Loveless and A. L. Garner, Scaling laws for gas breakdown for nanoscale to microscale gaps at atmospheric pressure, Appl. Phys. Lett. **108**, 234103 (2016).
[16] V. Vahedi, C. K. Birdsall, M. A. Lieberman, G. DiPeso, and T. D. Rognlien, Verification of frequency scaling laws for capacitive radio-frequency discharges using two-dimensional simulations, Phys. Fluids B **5**, 2719 (1993).
[17] S. Wilczek, J. Trieschmann, J. Schulze, E. Schuengel, R. P. Brinkmann, A. Derzsi, I. Korolov, Z. Donkó, and T. Mussenbrock, The effect of the driving frequency on the confinement of beam electrons and plasma density in low-pressure capacitive discharges, Plasma Sources Sci. Technol. **24**, 024002 (2015).
[18] S. Sharma, A. Sen, N. Sirse, M. M. Turner, and A. R. Ellingboe, Plasma density and ion energy control via driving frequency and applied voltage in a collisionless capacitively coupled plasma discharge, Phys. Plasmas **25**, 080705 (2018).
[19] T. Kikuchi and S. Kogoshi, Dependence of plasma density on driving frequency in conventional capacitively coupled discharges at higher frequencies, Jpn. J. Appl. Phys. **42**, 4290 (2003).
[20] M. Vass, S. Wilczek, T. Lafleur, R. P. Brinkmann, Z. Donkó, and J. Schulze, Observation of dominant ohmic electron power absorption in capacitively coupled radio frequency argon discharges at low pressure, Plasma Sources Sci. Technol. **29**, 085014 (2020).
[21] K. Zhao, D.-Q. Wen, Y.-X. Liu, M. A. Lieberman, D. J. Economou, and Y.-N. Wang, Observation of nonlinear standing waves excited by plasma-series-resonance-enhanced harmonics in capacitive discharges, Phys. Rev. Lett. **122**, 185002 (2019).
[22] J. Schulze, A. Derzsi, K. Dittmann, T. Hemke, J. Meichsner, and Z. Donkó, Ionization by drift and ambipolar electric fields in electronegative capacitive radio frequency plasmas, Phys. Rev. Lett. **107**, 275001 (2011).
[23] J. S. Townsend, *Electricity in Gases* (British Institute of Radiology, London, 1915).
[24] R. Holm, Zur Theorie des Glimmstromes, in *Wissenschaftliche Veröffentlichungen aus dem Siemens-Konzern: III. Band*, edited by C. D. Harries (Springer, Berlin. Heidelberg, 1923), pp. 159–189.
[25] A. von Engel, *Ionized Gases*, 2nd ed. (Clarendon, Oxford, UK, 1965).
[26] H. Margenau, Theory of high frequency gas discharges. IV. Note on the similarity principle, Phys. Rev. **73**, 326 (1948).
[27] E. I. Gordon and A. D. White, Similarity laws for the effects of pressure and discharge diameter on gain of He–Ne lasers, Appl. Phys. Lett. **3**, 199 (1963).
[28] C. E. Muehe, Scaling laws for high-density plasmas, J. Appl. Phys. **45**, 82 (1974).
[29] V. P. Kalanov, V. M. Milenin, G. J. Panasjuk, and N. A. Timofeev, Similarity rules for low-pressure gas discharges in a metal + rare gas mixture, Phys. Lett. A **126**, 336 (1988).
[30] C. Wilke, B. P. Koch, and B. Bruhn, Scaling laws and nonlinear wave dynamics in neon glow discharges, Phys. Plasmas **12**, 033501 (2005).
[31] Y. Fu, H. Luo, X. Zou, and X. Wang, Cathode fall thickness of abnormal glow discharges between parallel-plane electrodes in different radii at low pressure, Phys. Plasmas **22**, 023502 (2015).
[32] D. Michael, M. Khodorkovskii, A. Pastor, N. Timofeev, and G. Zissis, Application of similarity laws as a light source diagnostics, J. Phys. D **43**, 234005 (2010).
[33] N. Liu and V. P. Pasko, Effects of photoionization on similarity properties of streamers at various pressures in air, J. Phys. D **39**, 327 (2006).
[34] T. M. P. Briels, E. M. van Veldhuizen, and U. Ebert, Positive streamers in air and nitrogen of varying density: Experiments on similarity laws, J. Phys. D **41**, 234008 (2008).
[35] G. A. Mesyats, Similarity laws for pulsed gas discharges, Phys. Usp. **49**, 1045 (2006).
[36] P. Osmokrovic, T. Zivic, B. Loncar, and A. Vasic, The validity of the general similarity law for electrical breakdown of gases, Plasma Sources Sci. Technol. **15**, 703 (2006).
[37] D. Yang, J. P. Verboncoeur, and Y. Fu, Demonstration of similarity laws and scaling networks for radio-frequency plasmas, Phys. Rev. Lett. **134**, 045301 (2025).
[38] Y. Fu and J. P. Verboncoeur, On the similarities of low-temperature plasma discharges, IEEE Trans. Plasma Sci. **47**, 1994 (2019).
[39] Y. Fu, B. Zheng, P. Zhang, Q. H. Fan, J. P. Verboncoeur, and X. Wang, Similarity of capacitive radio-frequency discharges in nonlocal regimes, Phys. Plasmas **27**, 113501 (2020).
[40] Y. Fu, B. Zheng, D.-Q. Wen, P. Zhang, Q. H. Fan, and J. P. Verboncoeur, Similarity law and frequency scaling in low-pressure capacitive radio frequency plasmas, Appl. Phys. Lett. **117**, 204101 (2020).
[41] D. Yang, H. Wang, B. Zheng, X. Zou, X. Wang, and Y. Fu, Application of similarity laws to dual-frequency capacitively coupled radio frequency plasmas with the electrical asymmetry effect, Plasma Sources Sci. Technol. **31**, 115002 (2022).
[42] Y. Fu, H. Wang, B. Zheng, P. Zhang, Q. H. Fan, X. Wang, and J. P. Verboncoeur, Generalizing similarity laws for radio-frequency discharge plasmas across nonlinear transition regimes, Phys. Rev. Appl. **16**, 054016 (2021).
[43] D. Yang, H. Wang, B. Zheng, X. Zou, X. Wang, and Y. Fu, Scale-invariant resonance characteristics in magnetized capacitive radio frequency plasmas, Phys. Plasmas **30**, 063510 (2023).

[44] C. J. Mogab, A. C. Adams, and D. L. Flamm, Plasma etching of Si and SiO_2—the effect of oxygen additions to CF_4 plasmas, J. Appl. Phys. **49**, 3796 (1978).

[45] A. Efremov, J. Lee, and K.-H. Kwon, A comparative study of CF_4, Cl_2 and HBr+Ar inductively coupled plasmas for dry etching applications, Thin Solid Films **629**, 39 (2017).

[46] C. Wang, B. Zhang, S. Chen, Y. Sun, X. Yang, Y. Peng, X. Chen, and G. Zhang, Surface modification of silicone rubber by CF_4 radio frequency capacitively coupled plasma for improvement of flashover, Plasma Sci. Technol. **24**, 025501 (2022).

[47] S.-H. Gao, K.-S. Zhou, M.-K. Lei, and L.-S. Wen, Surface modification of silicone rubber by CF_4 radio frequency plasma immersion, Plasma Chem. Plasma Proc. **28**, 715 (2008).

[48] Y. X. Liu, E. Schungel, I. Korolov, Z. Donkó, Y. N. Wang, and J. Schulze, Experimental observation and computational analysis of striations in electronegative capacitively coupled radio-frequency plasmas, Phys. Rev. Lett. **116**, 255002 (2016).

[49] Y.-X. Liu, I. Korolov, E. Schüngel, Y.-N. Wang, Z. Donkó, and J. Schulze, Striations in electronegative capacitively coupled radio-frequency plasmas: Analysis of the pattern formation and the effect of the driving frequency, Plasma Sources Sci. Technol. **26**, 055024 (2017).

[50] D. Yang, X. Wang, Z. Zhou, H. Li, W. Zhang, Y. Liu, J. Schulze, P. Hartmann, Z. Donkó, and Y. Fu, Discharge similarity in capacitive radio frequency carbon tetrafluoride plasmas, Appl. Phys. Lett. **127**, 124101 (2025).

[51] Y. Fu, H. Wang, and X. Wang, Similarity theory and scaling laws for low-temperature plasma discharges: A comprehensive review, Rev. Mod. Plasma Phys. **7**, 10 (2023).

[52] A. Von Engel and M. Steenbeck, *Elektrische Gasentladungen: Ihre Physik und Technik* (Springer, Berlin, 1932).

[53] D. Yang, Y. Fu, B. Zheng, H. Wang, Q. H. Fan, X. Zou, X. Wang, and J. P. Verboncoeur, Similarity properties in capacitive radio frequency plasmas with nonlinear collision processes, Plasma Sources Sci. Technol. **30**, 115009 (2021).

[54] X.-K. Wang, R. Masheyeva, Y.-X. Liu, P. Hartmann, J. Schulze, and Z. Donkó, The electrical asymmetry effect in electronegative CF_4 capacitive RF plasmas operated in the striation mode, Plasma Sources Sci. Technol. **32**, 085009 (2023).

[55] A. V. Phelps, The application of scattering cross sections to ion flux models in discharge sheaths, J. Appl. Phys. **76**, 747 (1994).

[56] R. Masheyeva, M. Vass, X.-K. Wang, Y.-X. Liu, A. Derzsi, P. Hartmann, J. Schulze, and Z. Donkó, Electron power absorption in CF_4 capacitively coupled RF plasmas operated in the striation mode, Plasma Sources Sci. Technol. **33**, 045019 (2024).

[57] D. Yang, Y. Fu, Z. Liu, X. Han, and Y. Fu, Kinetic simulations of hollow cathode discharge and its interactions with different target materials, IEEE Trans. Plasma Sci. **52**, 4520 (2024).

[58] Z. Zhou, X. Wang, H. Li, D. Yang, W. Zhang, J. Schulze, P. Hartmann, Z. Donkó, Y. Liu, and Y. Fu, Dynamics of electron power absorption in capacitive radio-frequency CF_4 plasmas operating in the striation mode, Plasma Sources Sci. Technol. **34**, 085014 (2025).